Numerical Simulation of Geothermal Well Testing Under Near and Supercritical Conditions: Preliminary Results

Jorge Alberto Rangel Arista*[1], Sadiq J. Zarrouk, and Saeid Jalilinasrabady[2]

[1] Department of Engineering Science and Biomedical Engineering, The University of Auckland, Private Bag, 92019, Auckland 1142, New Zealand.

[2] Earth Science New Zealand, PO Box 30-368, Wellington, New Zealand.

*[1]jran489@aucklanduni.ac.nz

Keywords: *Supercritical, Geothermal well testing, PTA, TTA*

ABSTRACT

Geothermal power capacity has grown steadily over recent decades; however, many of the most accessible geothermal resources have already been developed. Deep geothermal resources under existing conventional systems, particularly those at depths of approximately 4,000 to 5,000 m, represent a substantial untapped energy resource. Their commercial development remains challenging due to high drilling costs and extreme temperature and pressure conditions, which increase technical and investment risks. Robust characterisation of well–reservoir interactions is therefore essential. Pressure Transient Analysis (PTA) and Temperature Transient Analysis (TTA) can provide valuable insights into reservoir behaviour, although their application under supercritical conditions is not yet well established. This study uses numerical simulation to investigate geothermal well testing under near and supercritical conditions. It proposes a practical approach to analysing these systems and identifies the key parameters that influence pressure and temperature responses. The results indicate that at a high reservoir pressure of 400 bar, despite the complex fluid behaviour associated with supercritical conditions, the transient responses retain several features comparable to those of conventional geothermal well tests. These preliminary findings support the potential adaptation of established well-test interpretation methods for deep, high-temperature geothermal resources.

1. INTRODUCTION

Geothermal energy is one of the most promising renewable energy resources, with substantial capacity and significant potential for further development (Grant & Bixley, 2011; Zarrouk & McLean, 2019). However, many shallow, readily accessible geothermal fields have already been developed. A considerable proportion of the remaining geothermal resource is located at depths greater than approximately 3,500 m, where reservoirs may experience extremely high temperatures and pressures, including supercritical conditions. These environments offer the potential for high energy output but present major technical and commercial challenges.

Several international projects have investigated deep and supercritical geothermal resources, including the Iceland Deep Drilling Project, the Japan Beyond Brittle Project, the DESCRAMBLE project in Italy, the Hotter and Deeper project in the Taupō Volcanic Zone of New Zealand, projects at The Geysers and Salton Sea in the United States, and the GEMex project in Mexico (Dobson et al., 2017). Exploration activities at several of these sites have encountered, or sought to access, supercritical reservoir conditions. However, drilling and operating under such conditions remain difficult because extreme temperatures can reduce the performance and durability of drilling equipment, well casings, cement, and other downhole components.

Numerical simulation is therefore essential for investigating the behaviour of deep geothermal reservoirs and reducing the technical and financial risks associated with their development. Several studies have developed numerical formulations and simulation tools for modelling water and fluid flow under supercritical conditions, including Hayba and Ingebritsen (1994), Yano and Ishido (1998), Ingebritsen et al. (2010), and Croucher and O'Sullivan (2008). These studies established important foundations for representing the strongly nonlinear thermophysical behaviour of water near and above the critical point.

Despite these advances, most geothermal well testing studies have focused on subcritical reservoir conditions (McLean & Zarrouk, 2017; Adiputro et al., 2020; Rangel-Arista et al., 2024). Consequently, established Pressure Transient Analysis methods may not be directly applicable to supercritical systems, where fluid density, viscosity, compressibility, and other properties can change rapidly with pressure and temperature. Research examining well-test responses under supercritical conditions remains limited. Yano and Ishido (1998), for example, used one-dimensional numerical models in STAR and HOTH2O to simulate pressure drawdown and buildup over different production periods. Their results showed that pressure responses were strongly influenced by nonlinear variations in fluid kinematic viscosity and compressibility.

Geothermal well testing is a well-established method for evaluating reservoir properties and well performance. However, there is currently no widely accepted framework for interpreting pressure and temperature transient responses under supercritical conditions. This study addresses this gap by presenting an initial numerical approach to geothermal well testing in a supercritical reservoir. The work examines the characteristic pressure and temperature responses of the system and identifies the principal parameters controlling their behaviour. The results provide a foundation for developing more robust well-testing and interpretation methods for deep, high-temperature geothermal resources.

2. SUPERCRITICAL SYSTEMS

The critical point of pure water occurs at 373.95°C and 22.064 MPa, as shown in Figure 1. Above both the critical temperature and critical pressure, the distinction between liquid and vapour disappears, and water exists as a single supercritical phase. In natural geothermal systems, dissolved salts can increase the critical temperature and pressure. However, the present study considers pure water and therefore uses its critical conditions throughout the analysis. The depth at which these conditions are encountered depends on the prevailing pressure and temperature gradients. Under a cold-water hydrostatic pressure regime, the critical pressure may be reached at a depth of approximately 2.3 km, although greater depths may be required for the temperature to exceed the critical temperature (Kruszewski and Wittig, 2018).

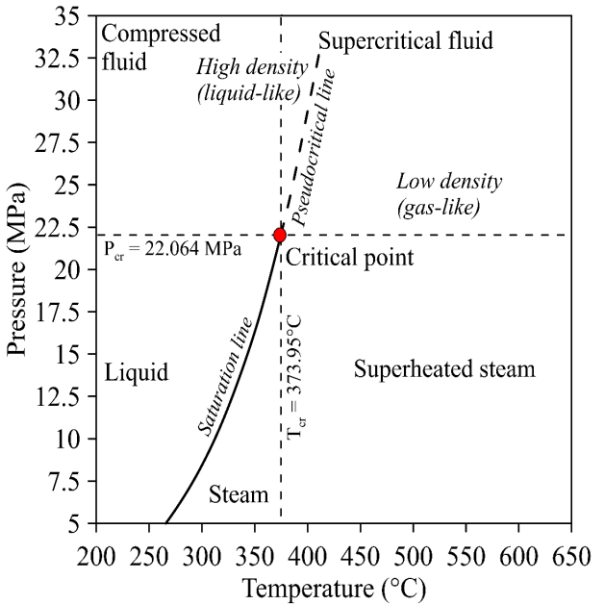


Figure 1: Phase diagram and critical point of water, adapted from Mokry et al. (2011).

Within the supercritical region, fluid properties vary continuously, without a distinct liquid-to-vapour phase boundary. This region can be divided into liquid-like and gas-like states by the pseudocritical line. At a given supercritical pressure, the pseudocritical temperature generally corresponds to the maximum isobaric heat capacity and the most rapid variation in several thermophysical properties. Below the pseudocritical temperature, supercritical water exhibits liquid-like behaviour, with relatively high density and strong solvent properties. Above the pseudocritical temperature, it becomes increasingly gas-like, with lower density, lower viscosity and reduced solvent capacity (Mokry et al., 2011). The transition across the pseudocritical line is continuous rather than a phase change, but the associated variations in fluid properties can be substantial.

Supercritical conditions strictly require both the temperature and pressure to exceed the critical values of water. If either parameter falls below its critical value, the fluid may enter a compressed liquid, two-phase saturated-steam, or superheated-steam state, depending on the corresponding pressure and temperature. During geothermal production, pressure and temperature may change significantly between the reservoir and the wellbore, allowing the fluid to traverse several thermodynamic regions.

Accurate representation of these thermodynamic regions is essential for modelling supercritical geothermal reservoirs and wells. The IAPWS-95 formulation provides the fundamental reference equation of state for the thermodynamic properties of pure water. In contrast, the IAPWS Industrial Formulation 1997, commonly referred to as IAPWS-IF97, was developed for computationally efficient engineering applications and closely approximates IAPWS-95. IAPWS-IF97 divides the thermodynamic domain into five regions: compressed liquid, superheated vapour, dense or supercritical fluid, the liquid–vapour saturation boundary and high-temperature vapour. Different fundamental equations are applied within each region to calculate properties such as density, specific enthalpy, heat capacity and sound speed.

The numerical simulations in this study use IAPWS-IF97 to calculate the properties of pure water as functions of pressure and temperature. This approach allows the model to represent conditions ranging from compressed water to supercritical states that are liquid-like and gas-like. Of particular importance are the rapid changes in density, viscosity, heat capacity, and compressibility near the pseudocritical line. These variations may influence fluid storage, pressure diffusivity and the resulting pressure-transient response, and must therefore be considered when interpreting well tests under supercritical conditions.

3. NUMERICAL CASE STUDY: SCW-1

3.1 Study objective and modelling framework

The modelling framework developed by Rangel-Arista et al. (2025) was applied to a hypothetical geothermal supercritical well (SCW-1), designated to compare pressure and temperature responses under near-critical and supercritical conditions. The framework combines Pressure Transient Analysis (PTA) and Transient Temperature Analysis (TTA), allowing the pressure and temperature responses generated during the well test to be analysed simultaneously.

3.2 Numerical simulator

The simulations were performed using the supercritical version of AUTOUGH2 (Croucher & O'Sullivan, 2008), a geothermal reservoir simulator based on TOUGH2 (Pruess et al., 2012). The supercritical formulation allows the properties of pure water to be calculated over a range of thermodynamic conditions, including compressed liquid, near critical, and supercritical states.

The thermophysical properties of pure water were calculated using the IAPWS-IF97 formulation. This enabled consistent calculation of properties such as density, viscosity, enthalpy, heat capacity and compressibility across the simulated pressure and temperature ranges.

PyTOUGH was used to generate and manage the AUTOUGH2 model files, execute simulations, and process numerical outputs. PyTOUGH comprises a series of Python scripts developed to facilitate the construction, execution and analysis of TOUGH2-family simulations (Croucher, 2020).

3.3 Model geometry

The SW-1 reservoir was represented using a two-dimensional axisymmetric radial model comprising the wellbore, a near-well skin zone and the surrounding reservoir. The numerical grid consists of multiple cylindrical blocks that increase logarithmically in size with radial distance from the well, as shown in Figure 2.

The well has a radius of 0.155 m and an effective wellbore volume of 120 m³. The assigned volume represents wellbore storage within the numerical model rather than the geometric volume calculated directly from the well radius and reservoir thickness.

The skin zone extends from the wellbore to a radius of 6 m, while the reservoir extends to an outer radius of 20,000 m. An open boundary was assigned at the outer edge of the model to allow pressure communication with the surrounding reservoir and reduce the influence of boundary effects on the simulated transient response.

The model comprises three vertical layers. The upper and lower matrix layers are each 100 m thick, and a 1 m thick higher-permeability fracture layer is positioned between them. The total modelled reservoir thickness is therefore 201 m.

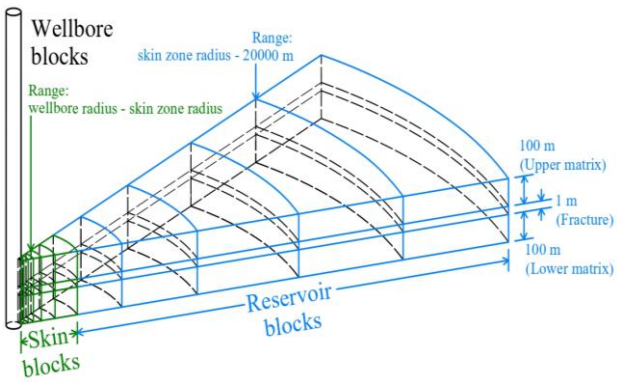


Figure 2: Radial grid geometry of the hypothetical SCW-1 reservoir.

3.4 Reservoir properties and assumptions

SCW-1 represents a simplified, laterally extensive geothermal reservoir without internal sealing boundaries, faults, or additional discrete fractures. The central 1 m thick fracture layer is the only explicitly represented high-permeability flow pathway.

The intrinsic permeability of the upper and lower matrix layers was set to 1 mD, while the fracture-layer permeability was set to 10 mD. The corresponding porosities were 0.01 for the matrix layers and 0.05 for the fracture layer. These values represent the relatively low porosity and permeability expected in deep geothermal rocks and are consistent with the ranges predicted by Solms et al. (2026).

Within the 6 m skin zone, the permeability of all three layers was increased to 100 mD. Because this permeability is higher than that of both the matrix and fracture layers, the skin zone represents an enhanced near-well region with negative skin. It may therefore be interpreted as a stimulated zone that improves fluid communication between the well and the surrounding reservoir. The principal model parameters are summarised in Table 1.

Table 1: SCW-1model parameters.

Parameter	Value
Effective Well volume (m^3)	120
Fracture layer thickness (m)	1
Fracture layer permeability (mD)	10
Fracture layer porosity	0.05
Well radius (m)	0.155
Upper and lower matrix permeability (mD)	1
Upper and lower matrix porosity	0.01
Skin radius (m)	6
Skin permeability (mD)	100
Skin condition	Negative skin
Model radial extent (km)	20
Outer boundary	Open
Injection temperature (°C)	80
Number of layers	3
Number of blocks in skin zone per layer	40
Number of blocks in reservoir zone per layer	60
Rock Density (kg/m³)	2750
Rock specific heat capacity (J/kg °C)	1200
Rock thermal conductivity (W/m °C)	2.5
Rock compressibility (Pa^{-1})	10^{-10}

The 120 m^3 (Table 1) well volume reflects the subsurface liquid volume occupied by the deep wellbore, while the negative skin is what is commonly expected in conventional geothermal wells, as positive skin is not common with current drilling methods.

3.5 Injection and pressure-falloff schedule

The injection-rate history shown in Figure 3 was applied to generate pressure and temperature responses for PTA and TTA. The initial injection period consisted of three sequential injection steps at mass rates of 20, 30 and 40 kg/s. Each step was maintained for 7,200 s (2 h), giving a total stepped-injection period of 6 h.

Following the 40 kg/s step, the injection rate was reduced to 10 kg/s and maintained for 165,600 s (46 h). The reduction in injection rate caused the reservoir pressure to decline from the level reached during the higher-rate injection period. This interval is therefore referred to as a pressure-falloff period under continued injection.

Unlike traditional injection falloff test, in which the well is completely shut in, the mass rate in the present simulations remained at 10 kg/s. This is known as non-zero injection rate pressure falloff, which is widely used by the geothermal

ISSN 2703-4275

industry in high temperature wells "*as the heat up of the well during the test causes thermal expansion of the wireline, pivoting of the pressure profiles in the well, and also internal flows suppressed during injection can start flowing again*" These effects reduce the validity of the pressure falloff (Zarrouk and McLean, 2019). This will be more important for supercritical wells transient testing due to the very high temperatures, which can significantly reduce the time the Pressure-Temperature-Spinner tool can stay inside the geothermal well without cooling (non-zero injection rate). The pressure and temperature responses during this 46 h interval were used for the transient analyses.

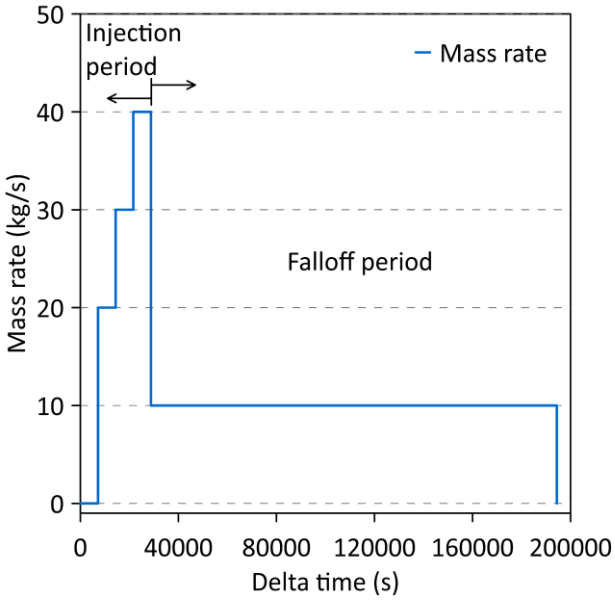


Figure 3: Stepped injection and pressure-falloff schedule under continued injection.

3.6 Simulated reservoir conditions

Six initial reservoir conditions were investigated, as summarised in Table 2. The initial reservoir pressure was fixed at 400 bar (40 MPa), while the initial temperature was increased from 350°C to 400°C in increments of 10°C.

Maintaining the same initial pressure for all six cases allowed the influence of reservoir temperature and thermodynamic state on the simulated pressure and temperature responses to be examined independently.

Table 2: Initial thermodynamic conditions of the SCW-1 simulation cases.

Case	Initial Pressure (bar)	Initial Temperature (°C)	Enthalpy (kJ/kg)
1	400	350	1588.1
2	400	360	1647.0
3	400	370	1709.4
4	400	380	1776.2
5	400	390	1849.2
6	400	400	1930.8

Cases 1 to 3 have pressures above the critical pressure of pure water but temperatures below its critical temperature of 373.95°C. These cases, therefore, represent high-pressure compressed-liquid conditions approaching the critical temperature.

Cases 4 to 6 exceed both the critical pressure and the critical temperature and, consequently, represent supercritical conditions. At 400 bar and temperatures between 380°C and 400°C, these cases remain within the liquid-like, or water-like, region of the supercritical domain shown in Figure 1.

The six cases, therefore, provide a controlled comparison between compressed water near the critical temperature and liquid-like supercritical water. The selected conditions do not extend across the pseudocritical line into the gas-like supercritical region.

3.7 Enthalpy and implications for geothermal production

At a constant pressure of 400 bar, the initial specific enthalpy increased from 1,588.1 kJ/kg at 350°C to 1,930.8 kJ/kg at 400°C (Table 2). This increase reflects the greater thermal energy carried by the fluid as the initial reservoir temperature increases.

The simulated specific enthalpies are lower than those of dry steam under typical geothermal production conditions, which may be approximately 2,800 kJ/kg. They may also be lower than the production enthalpies of some conventional high-temperature geothermal reservoirs. However, reservoir enthalpy alone is insufficient to determine the technical or economic performance of a geothermal well.

The power output of a well also depends on the production mass flow rate, wellbore pressure, heat losses, fluid expansion and flashing, surface separation conditions, conversion efficiency, and parasitic energy requirements. Nevertheless, a relatively low specific enthalpy may be particularly restrictive when combined with the low production rates that can occur in deep, low-permeability reservoirs. Under these conditions, both the energy carried per unit mass and the total mass flow rate may limit the power output of an individual well.

The temperature-entropy diagram presented in Figure 4 shows that increasing the supercritical reservoir temperature increases the fluid enthalpy. At comparable high temperatures, lower reservoir pressures may also be associated with higher specific enthalpies and different expansion characteristics. However, these conditions should not be automatically considered operationally preferable based solely on enthalpy. A complete assessment would require consideration of fluid exergy, reservoir deliverability, wellbore behaviour and surface power-generation performance.

3.8 Basis for the selected reservoir pressure

The initial reservoir pressure of 400 bar was selected as a hypothetical deep-reservoir condition rather than as a measured pressure for SCW-1. The Rotokawa geothermal

field in New Zealand was used as an indicative geological analogue when selecting this pressure.

The currently developed Rotokawa reservoir has a pressure of approximately 200 bar at a depth of around 2,000-2,500 m (Brun et al., 2021). On this basis, a greater pressure may reasonably be expected in a deeper reservoir at approximately 4,000 to 5,000 m.

However, this assumption does not imply that reservoir pressure increases linearly with depth. Pressure conditions in deep geothermal systems depend on the temperature-dependent fluid density, the pressure regime, permeability, geological structure, and the reservoir's hydraulic connectivity. The selected pressure of 400 bar should therefore be regarded as a plausible modelling assumption for comparing near-critical and supercritical behaviour, rather than as a prediction of the actual pressure beneath the Rotokawa geothermal field.

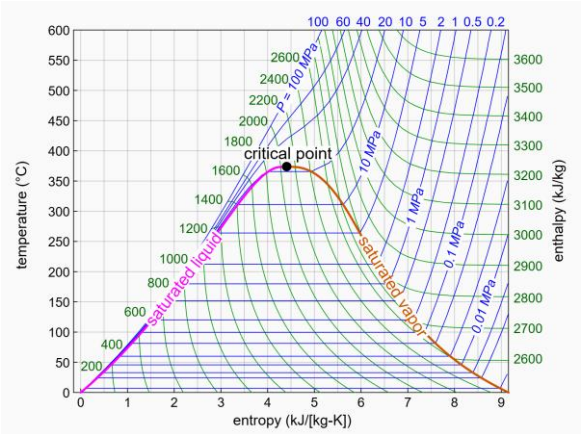


Figure 4: Temperature-entropy diagram for pure water, showing that the supercritical reservoir enthalpy increases with temperature, but decreases with increasing reservoir pressure (From thermodynamic-properties-phase-diagrams-interactive-simulations - LearnChemE).

4. RESULTS

4.1 Pressure and temperature responses

The pressure and temperature responses of the six cases were evaluated together with their corresponding derivatives. The pressure derivative was calculated using the method of Bourdet et al. (1983), while the temperature derivative was calculated following Onur et al. (2016). Both derivatives were calculated with respect to elapsed falloff time. Pressure and temperature were recorded in the numerical well block and therefore represent simulated wellbore conditions rather than undisturbed reservoir conditions.

4.1.1 Pressure response

After the third injection step, the injection mass rate was reduced from 40 to 10 kg/s, as shown in Figure 3. This reduction initiated a pressure-falloff response under continued injection. In all six cases, the well-block pressure initially decreased by approximately 30 bar before approaching a temporary stabilisation period, as shown in Figure 5.

The pressure subsequently rebounded by less than 2 bar because injection continued at 10 kg/s throughout the falloff period. Although the residual injection rate was substantially lower than the preceding rate of 40 kg/s, continued fluid entry into the low-permeability reservoir prevented an uninterrupted pressure decline.

The low matrix and fracture permeabilities restricted fluid transfer between the well and the surrounding formation. This caused substantial pressure accumulation during the stepped-injection period, with the well-block pressure increasing from the initial reservoir pressure of 400 bar to approximately 470 bar. The same low transmissivity also delayed the response when the injection rate was reduced.

The overall pressure declines and the rebounds were similar across all six cases, and no measurable difference was observed between the near-critical and supercritical cases. However, the time required to reach the temporary stabilisation period decreased as the initial reservoir temperature increased.

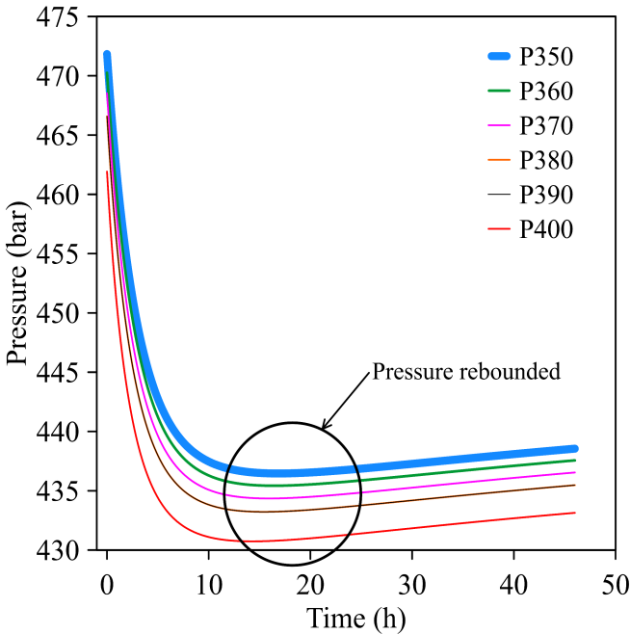


Figure 5: Simulated well-block pressure responses during the pressure-falloff period under continued injection. The pressure rebound has important implications for well-test design and interpretation because it modifies both the pressure response and the corresponding derivative. To obtain a clearer pressure-falloff response, the residual reinjection rate should be reduced as much as operationally practicable before the falloff period begins.

4.1.2 Pressure-derivative response

The pressure derivatives exhibited a non-standard response, as shown in Figure 6. At early time, the derivatives followed an approximately unit-slope trend for around 15 s. This behaviour is consistent with wellbore storage, during which the measured pressure response is dominated by fluid storage within the well rather than flow through the reservoir.

The early unit-slope response was followed by a short interval without the characteristic derivative hump

commonly associated with the transition from wellbore storage to formation-dominated flow (Zarrouk and McLean, 2019). This interval corresponded to the brief pressure stabilisation observed in Figure 5.

As the well-block pressure began to rebound, the pressure derivative became negative, producing a gap in the plotted derivative response that persisted for most of the remaining falloff period. None of the cases developed a clear horizontal derivative plateau associated with infinite-acting radial flow. Instead, the derivatives approached zero as the pressure responses became increasingly affected by continued injection.

The absence of an identifiable infinite-acting radial-flow regime was probably due to a combination of low reservoir permeability, the continued injection rate, the test duration, and the open outer boundary condition. As a result, conventional PTA interpretation could not be applied reliably to estimate reservoir transmissivity or skin from the simulated responses.

No measurable differences were observed between the pressure-derivative responses of the six initial reservoir conditions. The pressure-transient behaviour was therefore controlled predominantly by the model properties and injection schedule rather than by whether the initial fluid state was near-critical or supercritical.

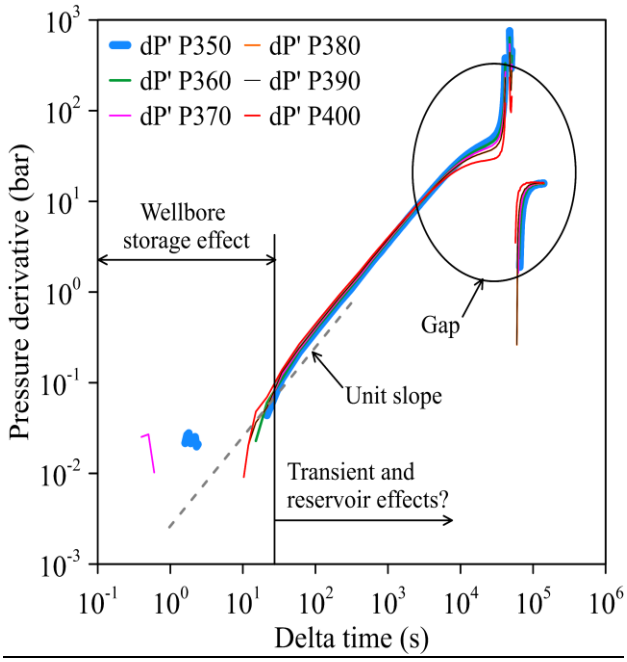


Figure 6: Pressure derivatives calculated with respect to elapsed falloff time.

4.1.3 Temperature response

The well-block temperatures continued to decrease after the injection rate was reduced from 40 to 10 kg/s. Because the injected water temperature was 80°C, substantially lower than the initial reservoir temperatures of 350–400°C, the simulated well-block temperatures decreased sharply and approached approximately 83–84°C during the falloff period, as shown in Figure 7.

These temperatures represent conditions within the numerical well block and should not be interpreted as reservoir temperatures. The well-block temperature was dominated by the continued injection of 80°C water. The high reservoir pressure may also have reduced the sensitivity of the well-block temperature response to differences in the initial reservoir temperature, effectively masking the thermal distinction between the six reservoir cases.

At the beginning of the falloff period, the well-block temperature decreased by a further approximately 6°C before reaching a first minimum or near-stabilisation point. The temperature then increased slightly before approaching a second temporary stabilisation point.

The times at which these stabilisation features occurred decreased as the initial reservoir temperature increased. However, the overall temperature-response shapes and magnitudes remained similar, and no measurable distinction was identified between the near-critical and supercritical cases.

The slight temperature increase was much less pronounced than the pressure rebound because continued injection maintained a supply of relatively cold water to the well block. The simulated temperature response therefore reflects the combined effects of residual cold-water injection, wellbore storage and heat exchange between the well and the surrounding reservoir.

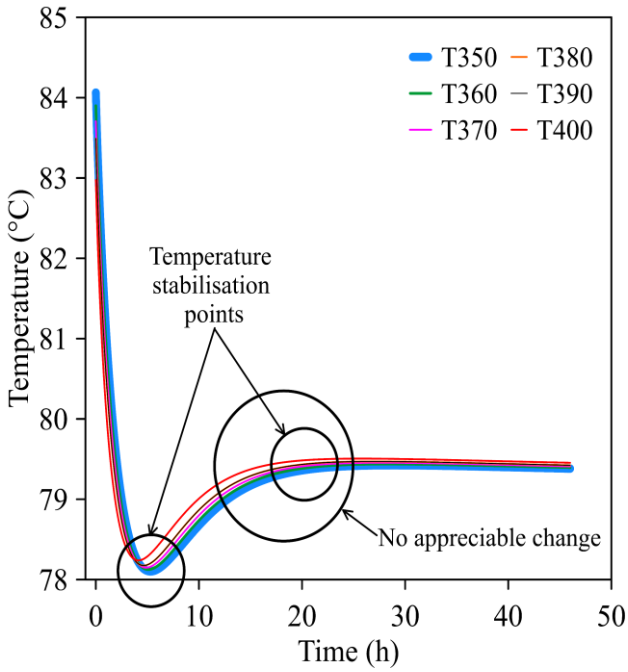


Figure 7: Simulated well-block temperature responses during the pressure-falloff period under continued injection.

4.1.4 Temperature-derivative response

The temperature derivatives exhibited a sequence of humps and troughs corresponding to changes in the slope of the temperature histories, as shown in Figure 8. An initial hump developed as the well-block temperature decreased rapidly. This feature represents the strong early-time cooling

response following the reduction in injection rate (Rangel-Arista et al., 2025).

The initial hump was followed by a downward trough associated with the first near-stabilisation point. As the rate of temperature change approached zero, the magnitude of the temperature derivative decreased. This feature corresponds to the first temporary stabilisation observed in Figure 7.

A second derivative hump subsequently developed as the well-block temperature increased slightly. This was followed by another downward trend as the temperature approached the second near-stabilisation point. The second sequence, therefore, reflects the minor thermal rebound and the subsequent reduction in the rate of temperature change.

As with the pressure responses, the derivative features occurred earlier as the initial reservoir temperature increased. Nevertheless, no measurable difference was observed in the overall form or magnitude of the temperature derivatives across the six cases.

The temperature derivatives were strongly influenced by the injection schedule and the measurement location within the well block. Rather than representing unrestricted thermal recovery towards the initial reservoir temperature, they primarily reflect the wellbore's response to continued injection of 80°C water and to heat exchange with the reservoir.

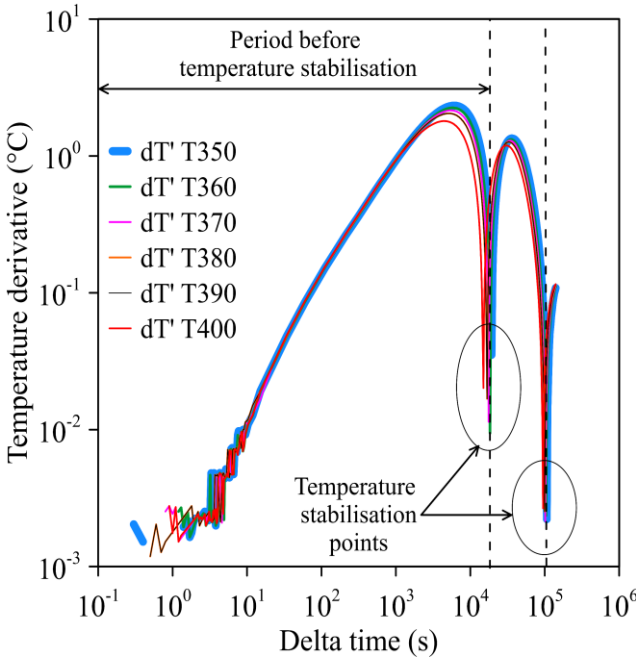


Figure 8: Temperature derivatives calculated with respect to elapsed falloff time.

4.1.5 Overall comparison

The six cases exhibited similar pressure, temperature and derivative responses despite spanning near-critical and liquid-like supercritical initial conditions. The principal difference was temporal: the pressure and temperature stabilisation features occurred earlier as the initial reservoir temperature increased. However, these timing differences were not accompanied by measurable changes in the overall response magnitude or derivative shape.

The results indicate that, under the conditions investigated, the transient response was dominated by the low reservoir permeability, effective wellbore storage, continued injection during the falloff period and the selected boundary conditions. These effects masked any clear distinction between the near-critical and supercritical cases.

The lack of an identifiable infinite-acting radial-flow regime also limited conventional PTA and TTA interpretation. Future pressure-falloff tests should therefore use the lowest practicable residual reinjection rate and, where operationally possible, a complete or near-complete shut-in. Reducing the reinjection rate would minimise the pressure rebound and provide a clearer transient response for evaluating reservoir properties.

5. CONCLUSIONS

The results indicate that, under the high-pressure supercritical conditions investigated, geothermal well-test responses may retain characteristics similar to those observed in conventional geothermal systems. The simulated cases covered conditions ranging from compressed-water states to water-like supercritical states. Within this range, the adapted numerical framework successfully simulated the hypothetical pressure and temperature responses, demonstrating its potential for further investigation of supercritical geothermal well testing. Although conditions shift from compressed to high-density (liquid-like) supercritical fluid (Figure 1, Table 2), thermodynamic differences remain minimal inside the well.

However, the findings are limited to the thermodynamic conditions considered in this study. Future work should examine additional scenarios, particularly conditions near the pseudocritical line, where fluid properties may change rapidly, and transitions from superheated-steam states to gas-like supercritical states. These conditions may produce more complex transient responses and require further development of interpretation methods.

In the cases investigated, maintaining the reservoir at high pressure resulted in lower production enthalpy than in the conventional subcritical reference case. This will reduce the energy available from the produced fluid, thereby limiting the commercial attractiveness of such operating conditions. Further studies are required to assess the trade-off between maintaining high reservoir pressure, preserving supercritical conditions, and maximising production enthalpy and overall energy recovery.

Future work will involve simulations with complete shut-in conditions, different permeability structure and boundary conditions and a wider range of supercritical (Pressure and Temperatures) states. Also, the framework will be used to investigate the impact of different stimulation methods, should the drilled well is of poor permeability.

ACKNOWLEDGEMENTS

This work was made possible through the New Zealand Ministry of Business, Innovation and Employment (MBIE) and the DeepHeat: unlocking superhot geothermal and national energy security through advanced permeability modelling (GNS2504).

REFERENCES

Acuna, J.A. (1994). Measurement of injectivity indexes in geothermal wells with two permeable zones. In: Proceedings, 19th Workshop on Geothermal Reservoir Engineering. Standford.

Bourdet, D., Whittle, T.M., Douglas, A.A., Pirard, Y.M., (1983). A new set of type curves simplifies well test analysis. World Oil 196 (6), 95–106.

Brun, Mo.L., Azwar, L. & Marsh, A. (2021). Using the Pressure While Drilling Data to Inform Drilling Decisions in the Kawerau and Rotokawa Geothermal Fields, NZ. Proceedings World Geothermal Congress 2020+1, Reykjavik, Iceland, April - October 2021

Croucher, A.: PyTOUGH user's guide. Department of Engineering Science, University of Auckland. (2020).

Croucher, A.E., & O'Sullivan, M.J.: Application of the computer code TOUGH2 to the simulation of supercritical conditions in geothermal systems, Geothermics, 37, (2008), 622–634.

Dobson, P., Asanuma, H., Huenges, E., Poletto, F., Reinsch, T. (2017). Supercritical Geothermal Systems - A Review of Past Studies and Ongoing Research Activities. 42nd Workshop on Geothermal Reservoir Engineering, Stanford, CA, United States.

Grant, M.A., Bixley, P.F., (2011). Geothermal Reservoir Engineering, 2nd ed. ELSEVIER.

Hayba, D.O., and Ingebritsen, S.E.: The computer model HYDROTHERM, a three-dimensional finite-difference model to simulate ground- water flow and heat transport in the temperature range of 0 to 1,200°C, U.S. Geological Survey Water-Resources Investigations Report, 94- 4045 (1994), 85 p.

IAPWS. (2018). Revised release on the IAPWS formulation 1995 for the thermodynamic properties of ordinary water substance for general and scientific use. The international association for the properties of water and steam.

Ingebritsen, S.E., Geiger, S., Hurwitz, S., & Driesner, T. (2010). Numerical simulation of magmatic hydrothermal systems. Reviews of Geophysics, 48, 33 p.

Kruszewski, M., Wittig, V., (2018). Review of failure modes in supercritical geothermal drilling projects. Geothermal Energy, 6(1).

McLean, K., & Zarrouk, S.J. (2015). Geothermal well test analysis using the pressure derivative: Some common issues and solutions. Geothermics. 55, 108–125.

Mokry, S., Pioro, I., Farah, A., King, K., Gupta, S., Peiman, W., Kirillov, P. (2011). Development of a supercritical water heat-transfer correlation for vertical bare tubes. Nuclear Engineering and Design, 241, 1126–1136.

Onur, M., Palabiyik, Y., Tureyen, O.I., Cinar, M., 2016. Transient temperature behaviour and analysis of single-phase liquid-water geothermal reservoirs during drawdown and buildup tests: Part II. Interpretation and analysis methodology with applications. J. Petrol. Sci. Engineer. 146, 657–669.

Pruess, K. TOUGH2 User's Guide, Version 2, Earth Sciences Division, Lawrence Berkeley National Laboratory University of California, Berkeley, California (2012)

Rangel-Arista, J. A., Zarrouk, S. J., & Kaya, E. (2025). Temperature transient analysis of a very high-permeability geothermal well: A numerical modelling approach. *Geothermics*, *127*, 103248.

Rangel-Arista, J. A., Zarrouk, S. J., Kaya, E., & Renderos Pacheco, R. E. (2023). Geothermal Temperature and Pressure Transient Analyses of Well CHI-8A, El Salvador During Pressure Falloff. Proceedings, 45th New Zealand Geothermal Workshop, Auckland, New Zealand.

Rangel-Arista, J. A., Zarrouk, S. J., Kaya, E., & Renderos Pacheco, R. E. (2025). Downflows during transient geothermal well test analysis. *Geothermics*, *125*, 103158.

Solms, T., Bachmanna, O., Chambefortb,I. & Driesnera, D. (2026). The potential for supercritical geothermal resources in the Taupō Volcanic Zone. Journal of Volcanology and Geothermal Research, VOLGEO 108687.

Yano, Y., Ishido, T., (1998). Numerical investigation of production behavior of deep geothermal reservoirs at super-critical conditions. Geothermics; 27(5-6): 705–721.

Zarrouk, S.J., McLean, K. (2019). Geothermal well test analysis: fundamentals, applications, and advanced techniques. ISBN: 9780128149461 Academic Press.